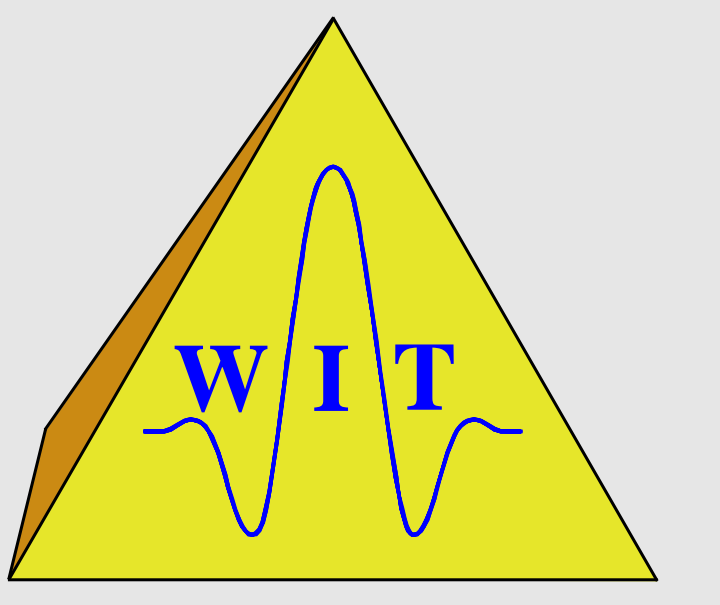


Common-Reflection-Surface Stack: a Macro-model-independent Seismic Imaging Method

Jürgen Mann, Thomas Hertweck, and Peter Hubral
Geophysical Institute, University of Karlsruhe, Germany



Summary

The common-reflection-surface (CRS) stack is a macro-velocity-model-independent method to simulate zero-offset (ZO) sections from multi-coverage seismic reflection data for 2-D media.

The CRS stacking operator depends on attributes of hypothetical wavefronts observed at the surface that allow to perform a subsequent inversion.

The CRS stacking operators fitting best to actual reflection events in the data set have to be determined by coherency analysis. The main task is the determination of these operators by variation of the attributes in a reasonable computation time preserving a sufficient accuracy.

Eigenwaves and wavefield attributes

The CRS stacking operator is based on wavefield attributes of two so-called *eigenwaves*. These eigenwaves are provided by the hypothetical experiments illustrated in Figure 1 for a model with three homogeneous layers.

A point source at depth point R provides the so-called *normal incidence point (NIP) wave* (Figure 1a), whereas an exploding reflector experiment yields the so-called *normal wave* (Figure 1b).

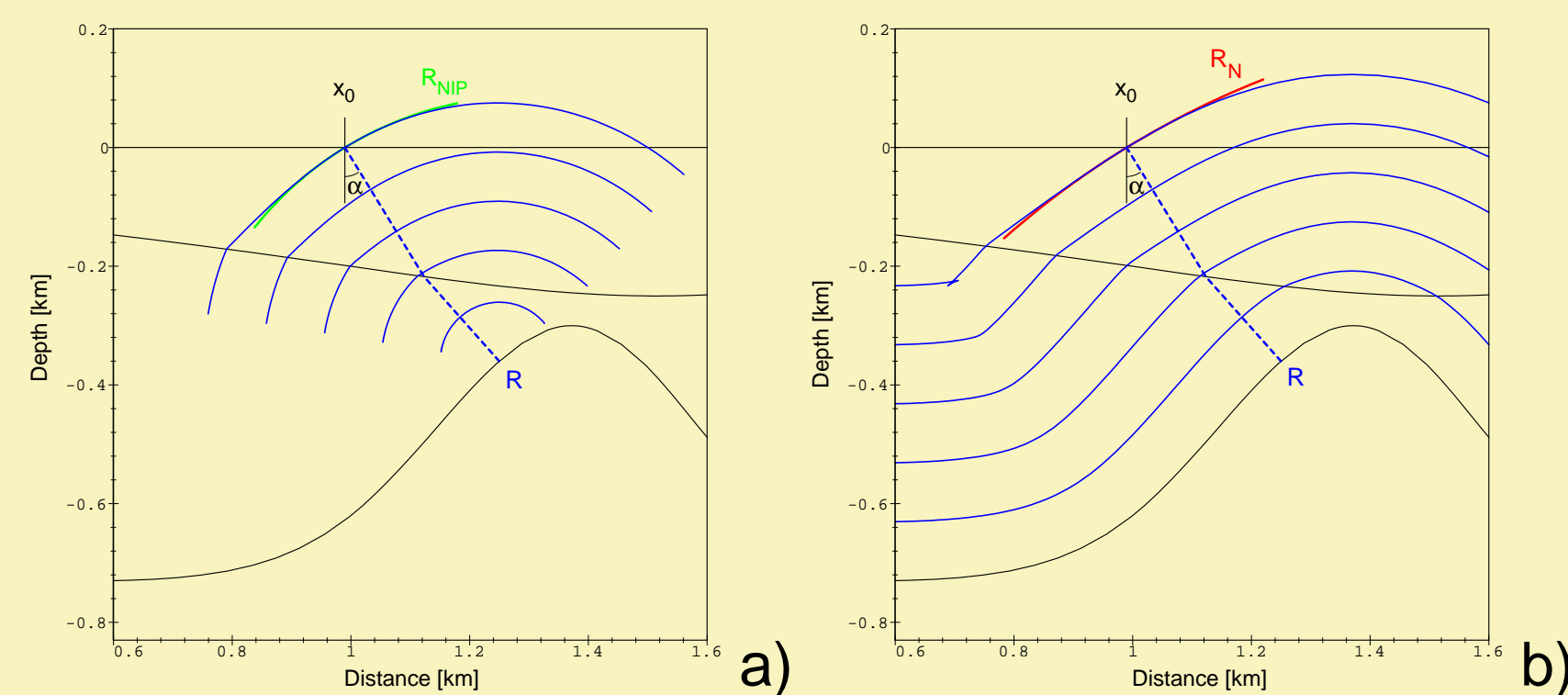


Figure 1: Two hypothetical experiments: a) *NIP* wave for a point source at R, b) *normal* wave for an exploding reflector. The central ray is shown as a dashed line.

A circular approximation of these wavefronts in a vicinity of x_0 at the surface can be represented by the following set of parameters:

- α , the angle of emergence of the central ray
- R_{NIP} , the radius of curvature of the *NIP* wave
- R_N , the radius of curvature of the *normal* wave

CRS stacking operator

The CRS stacking operator is given in a parametric form depending on the three wavefield attributes α , R_{NIP} , and R_N . Its more convenient hyperbolic Taylor expansion for a ZO location (t_0, x_0) reads

$$t^2(\Delta x, h) = \left(t_0 + \frac{2 \sin \alpha \Delta x}{v_0} \right)^2 + \frac{2 t_0 \cos^2 \alpha}{v_0} \left(\frac{\Delta x^2}{R_N} + \frac{h^2}{R_{NIP}} \right),$$

where v_0 denotes the near surface velocity, h the half offset, and Δx the distance between x_0 and the respective common midpoint (CMP).

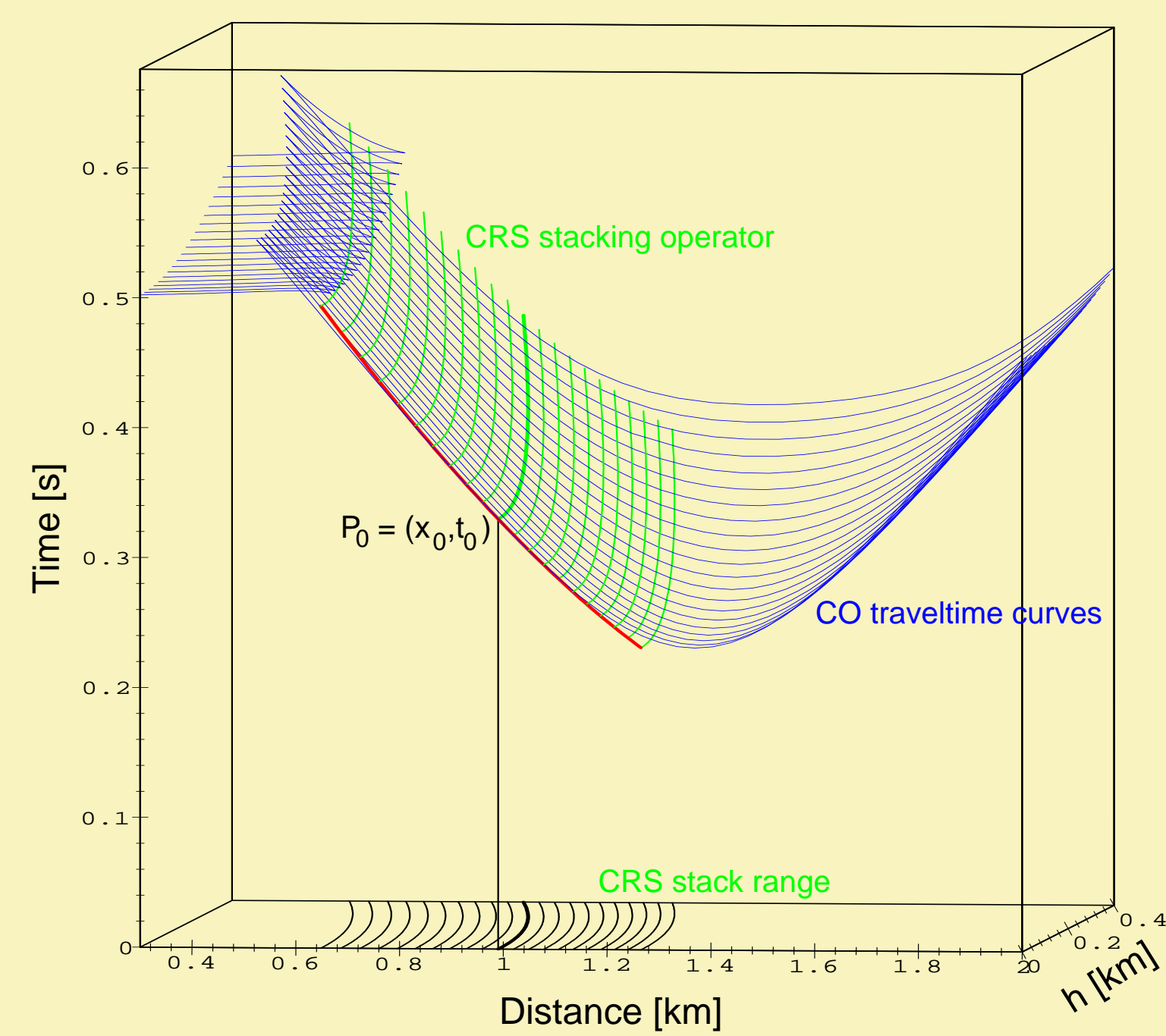


Figure 2: Forward calculated traveltimes surface (blue) compared to the CRS stacking operator (green) according to the true (model-derived) attributes. In the zero-offset plane the operator is depicted in red. The CRS stack range corresponds to a paraxial vicinity of the central ray.

Model

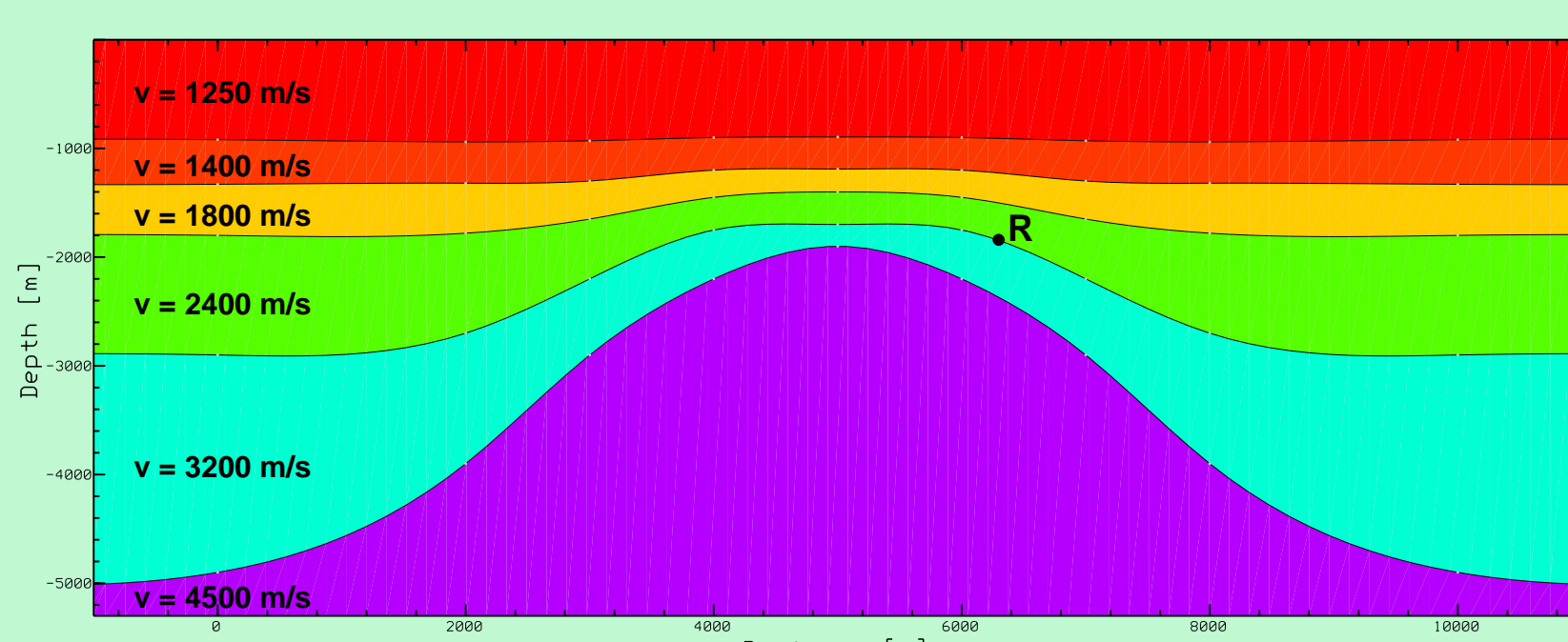


Figure 3: Model with homogeneous layers and dome-like interfaces. We simulated all primary events with a Ricker wavelet (30 Hz peak frequency) and a signal-to-noise ratio of 4.

Determination of the attributes

To determine the optimum stacking operator we look for the wavefield attributes yielding the highest coherency value along the respective operator in the multi-coverage data. Figure 4 illustrates the coherency in the three-parametric attribute domain for one selected point situated on an interface.

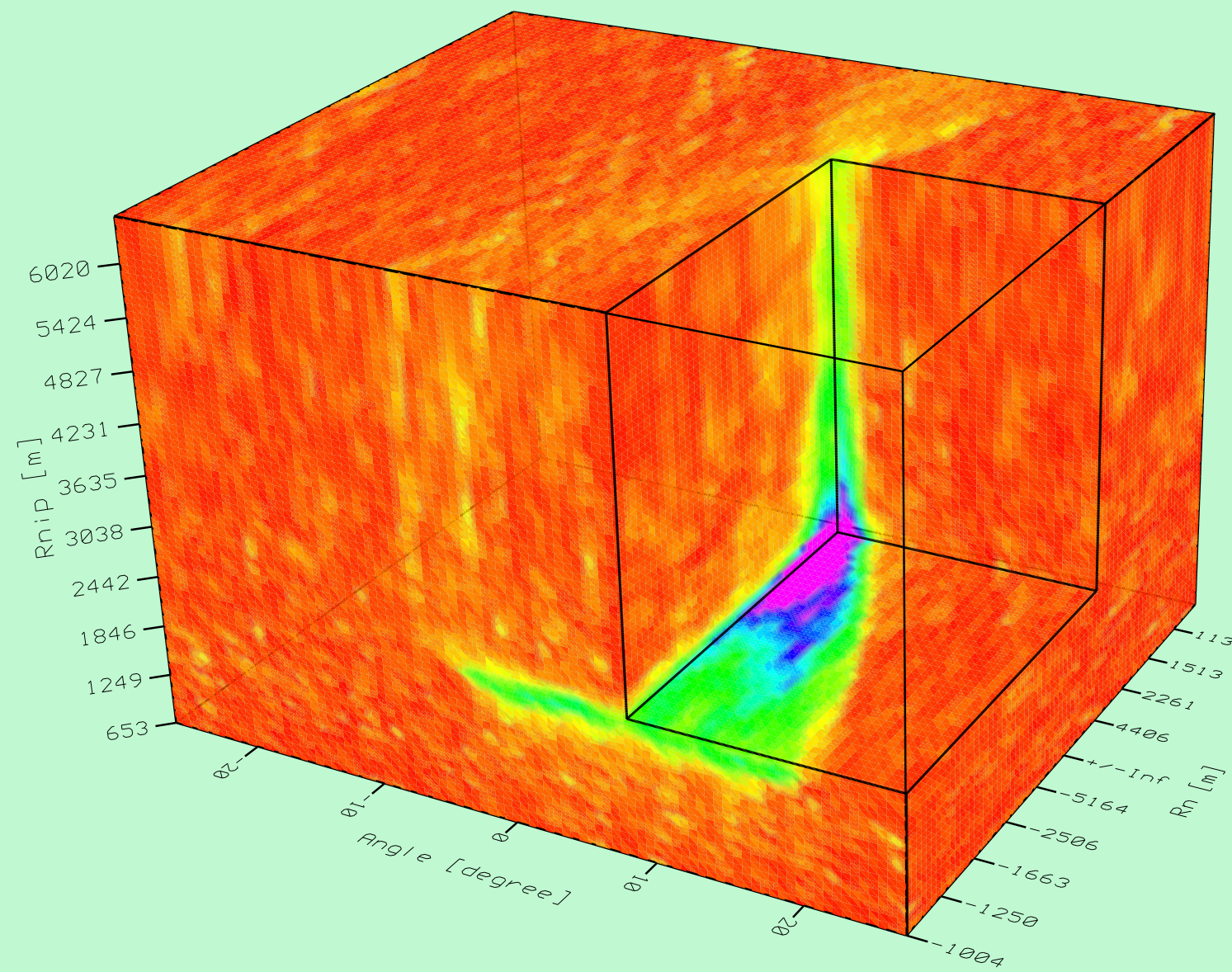


Figure 4: Coherency depending on the wavefield attributes for the depth point R depicted in Figure 3. The excavated block exposes the global maximum.

Due to the numerous local maxima, it would be extremely time consuming to perform a three-parametric global optimization for each ZO sample to be simulated. For a more efficient determination of the wavefield attributes we split the procedure into separate steps:

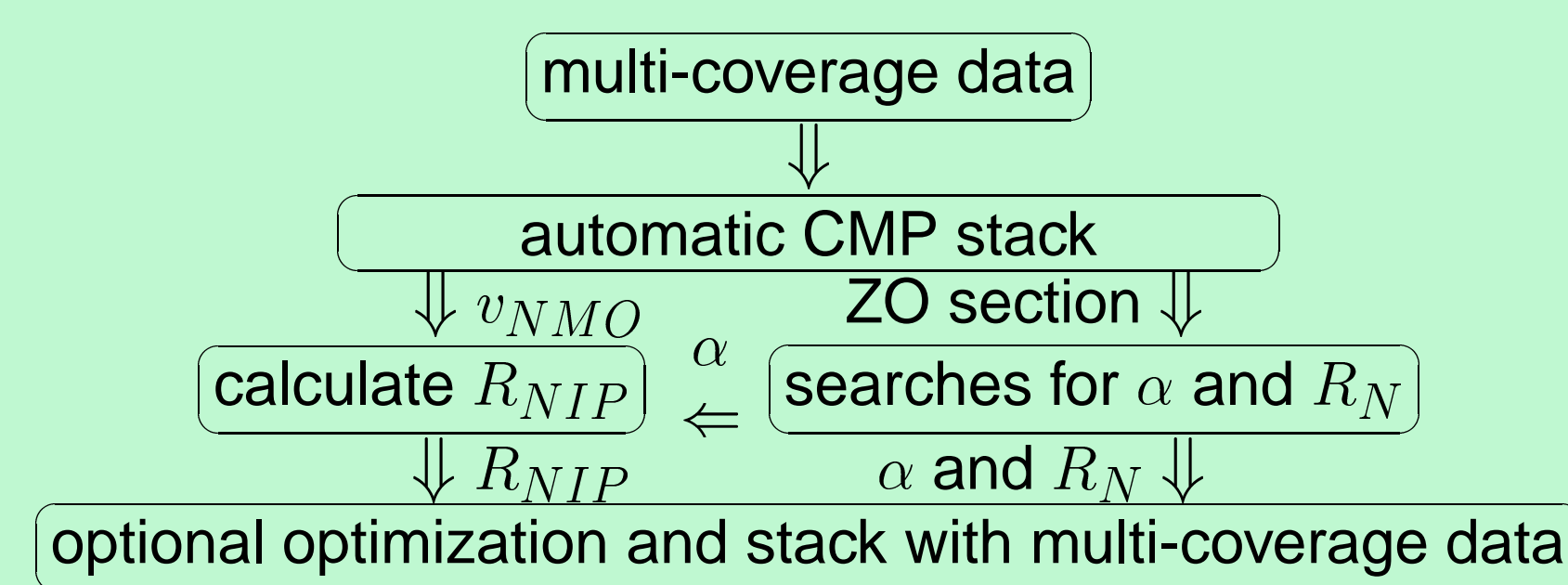


Figure 5: Simplified flowchart of the pragmatic approach to determine the wavefield attributes.

The automatic CMP stack is performed in the CMP gathers of the input data with a hyperbolic operator depending on the squared stacking velocity $v_{NMO}^2 = 2 v_0 R_{NIP} / (t_0 \cos^2 \alpha)$. We apply the subsequent searches for α and R_N to the result of the automatic CMP stack. The used operators are linear and hyperbolic, respectively. An optional local three-parametric optimization in the entire multi-coverage data serves to refine the wavefield attributes.

Simulated zero-offset section

The wavefield attributes determined by means of the pragmatic search strategy define the stacking operator in the multi-coverage data. The stacked section shown in Figure 6 is a kinematically correct ZO simulation. Due to the large number of contributing traces for each stacking operator, we obtain a high signal-to-noise ratio.

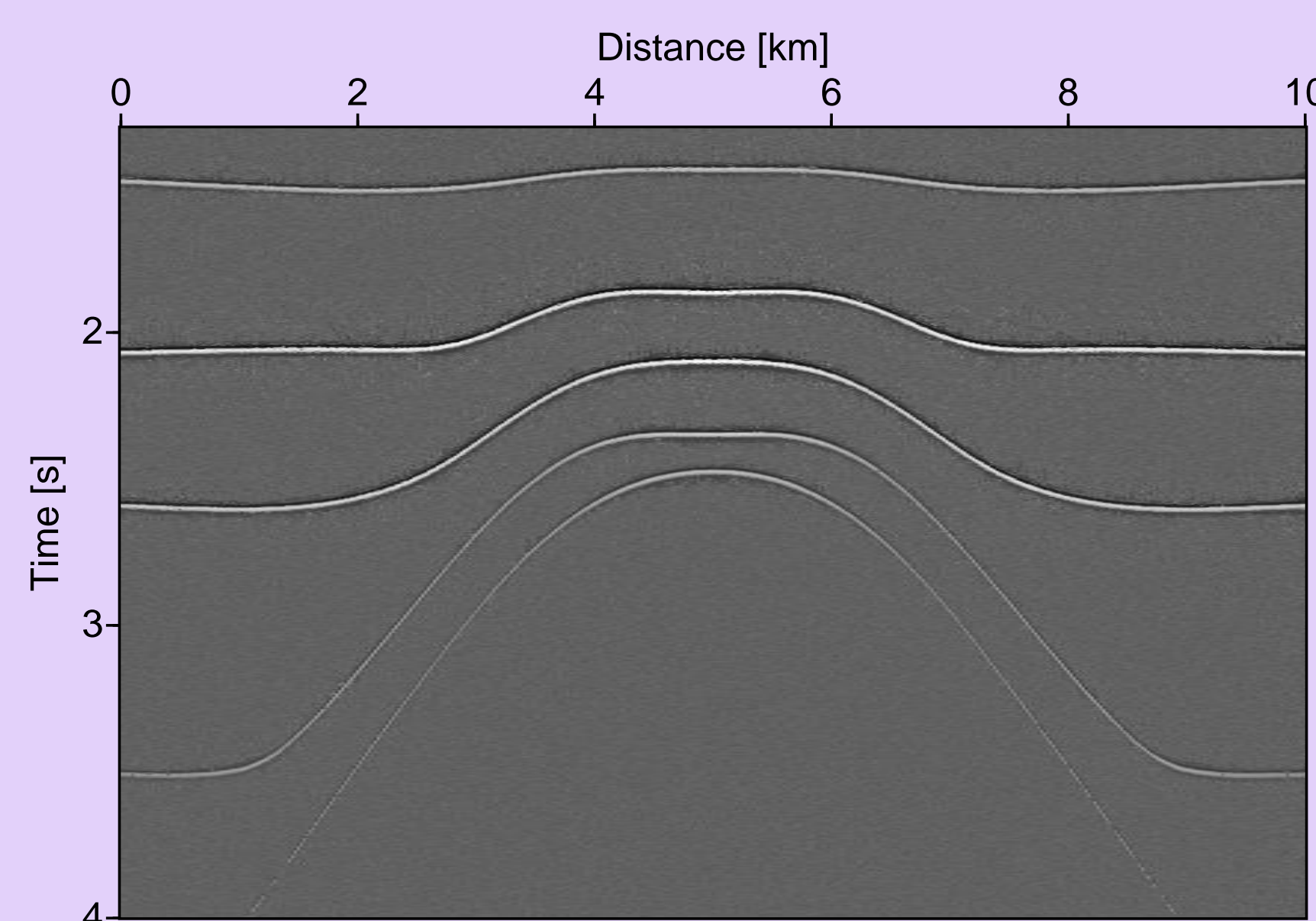


Figure 6: Stacked section as final result of the optimized CRS stack.

References

- Berkovitch, A., Gelchinsky, B., and Keydar, S., 1994, Basic formulae for multifocusing stack: 56th Mtg. Eur. Assoc. Expl. Geophys., Extended Abstracts, Session: P140.
- de Bazelaire, E., and Thore, P., 1987, Pattern recognition applied to time and velocity contours: 57th Annual Internat. Mtg., Soc. Expl. Geophys., Expanded Abstracts, Session: POS2.14.
- de Bazelaire, E., 1988, Normal moveout revisited – inhomogeneous media and curved interfaces: *Geophysics*, 53, no. 2, 143–157.
- Hubral, P., and Krey, T., 1980, Interval velocities from seismic reflection traveltimes measurements: *Soc. Expl. Geophys.*
- Schleicher, J., Tygel, M., and Hubral, P., 1993, Parabolic and hyperbolic paraxial two-point traveltimes in 3D media: *Geophys. Prosp.*, 41, no. 4, 459–513.

Model-derived vs. data-derived attributes

In addition to the stacked section in Figure 6, the CRS stack also provides a section for each of the three wavefield attributes α , R_{NIP} , and R_N . Thus, a set of wavefield attributes is available for each simulated ZO sample.

Instead of displaying the entire attribute sections, we extracted the data-derived wavefield attributes along the forward calculated traveltimes curves. This enables us to directly compare the data-derived attributes obtained from the CRS stack to their model-derived (forward calculated) counterparts:

Figure 7 and Figure 8 show the emergence angles and the radii of curvature of the *NIP* wave for all interfaces. For the sake of clarity, the radii of curvature of the *normal* wave in Figure 9 are shown separately for two interfaces.

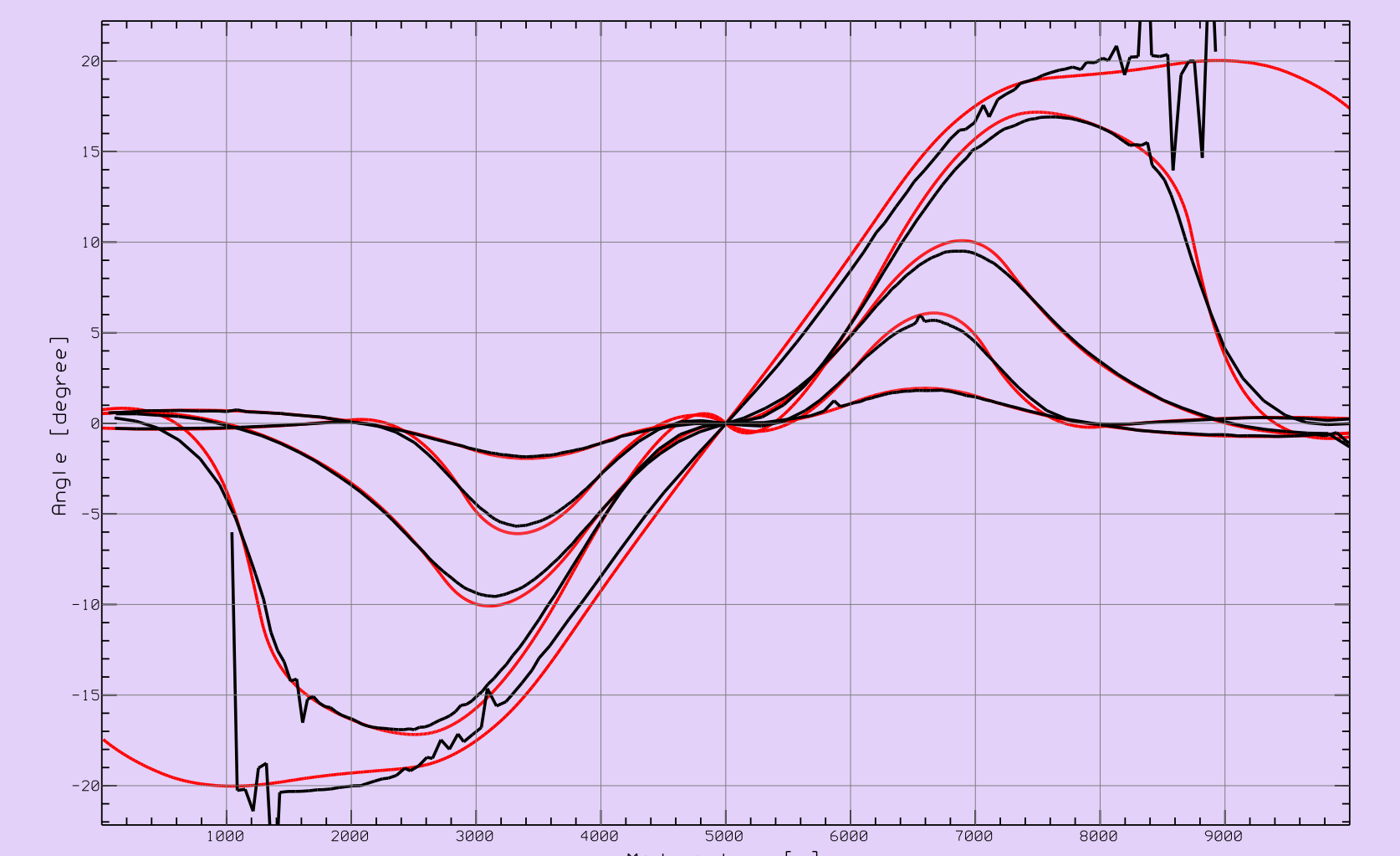


Figure 7: Model-derived (red) and data-derived (black) emergence angles for all layers.

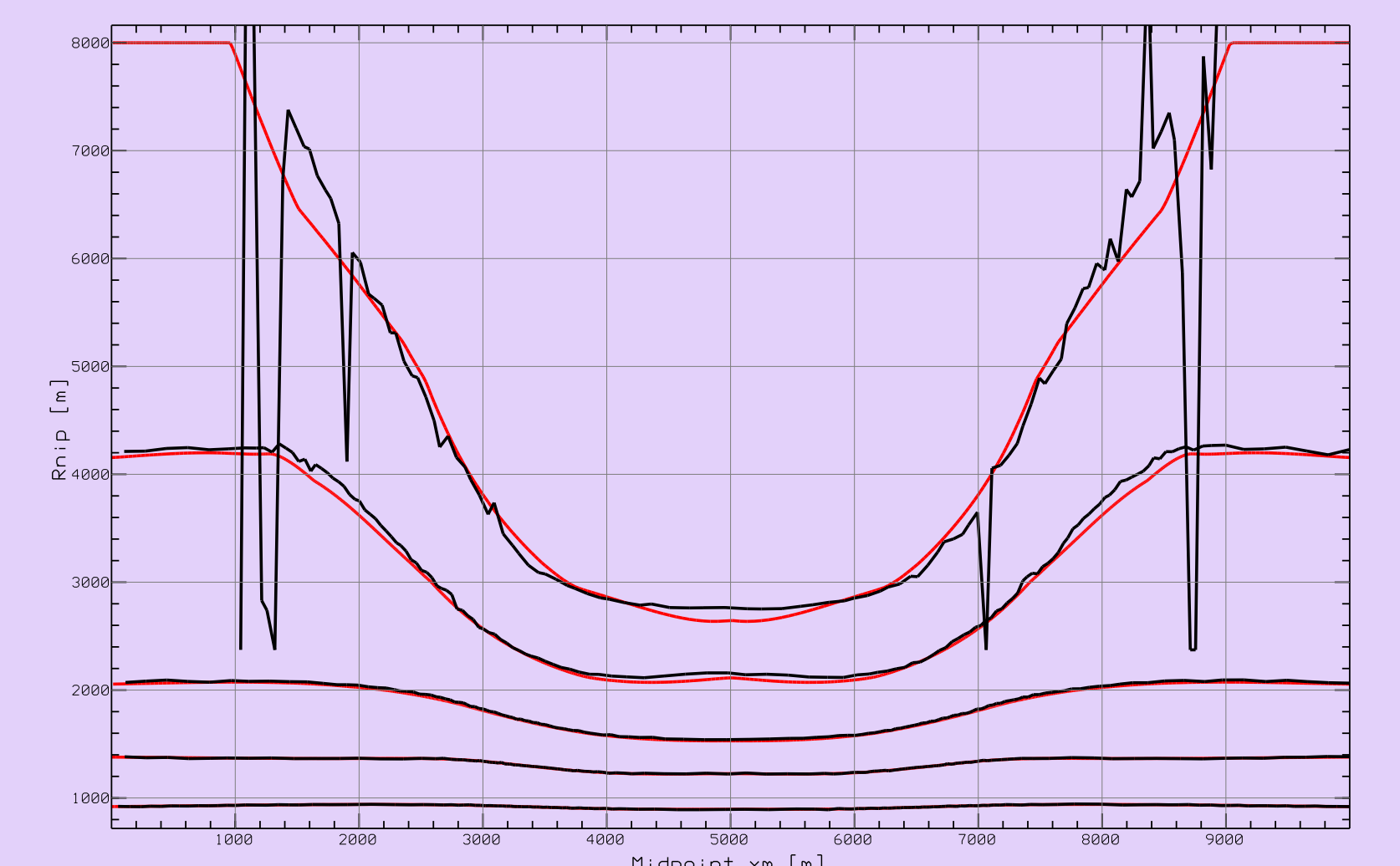


Figure 8: Model-derived (red) and data-derived (black) radii of curvature of the *NIP* waves for all layers.

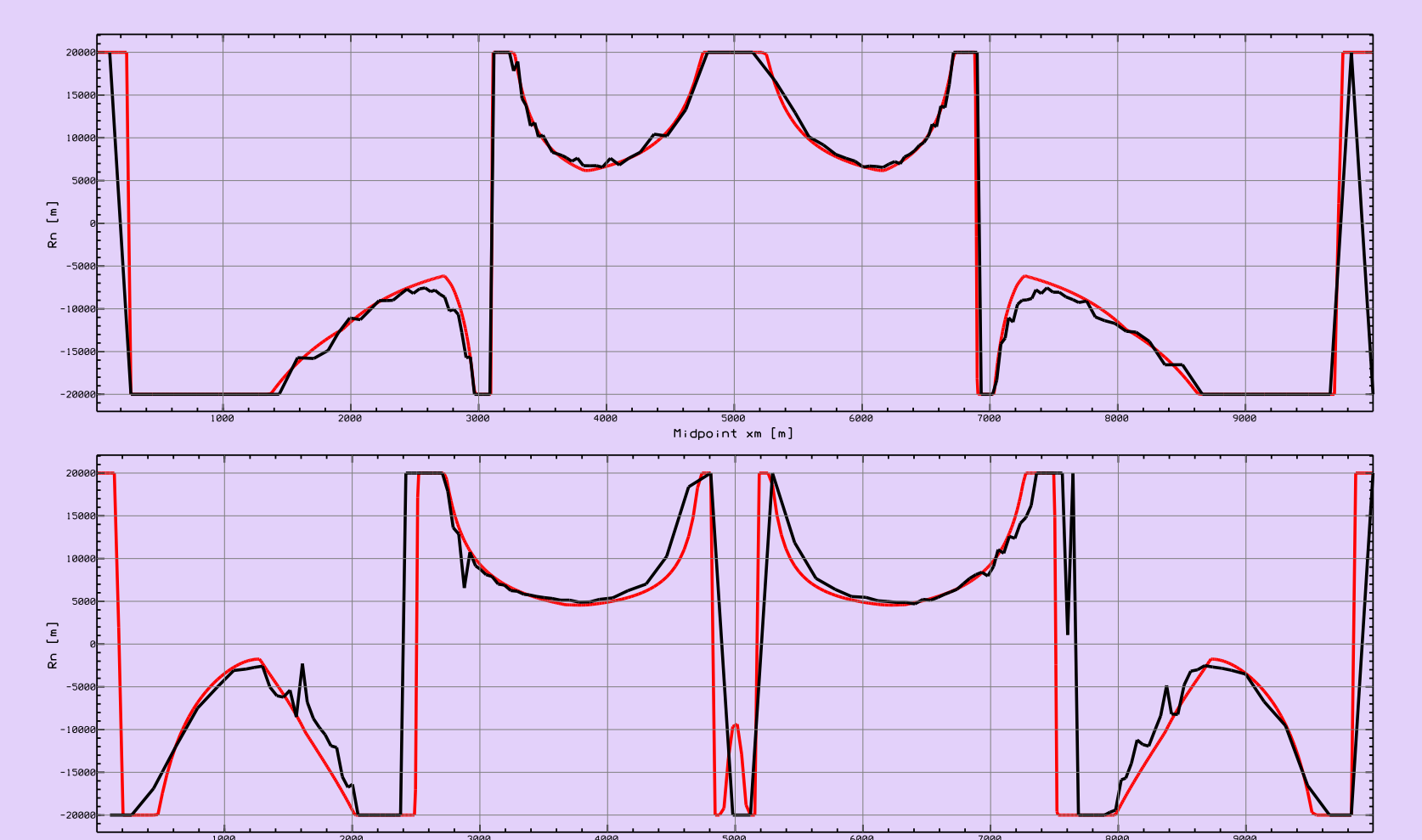


Figure 9: Model-derived (red) and data-derived (black) radii of curvature of the *normal* waves for the third and fourth interface.

We observe a wide agreement of the data-derived and the model-derived attributes. For the deepest interface we receive some deviations at the poorly illuminated flanks of the dome-like structure.

Conclusions

The CRS stack is a model-independent seismic imaging method and thereby can be performed without any ray tracing and macro velocity model estimation. Only the knowledge of the near surface velocity is required.

As a result of the CRS stack one obtains in addition to each simulated ZO sample important wavefield attributes: the angles of emergence and the radii of curvature of the *NIP* and the *normal* wave. With the proposed pragmatic search strategy we are able to recover a good approximation of the true, model-derived wavefield attributes.

The application to a synthetic dataset yielded noteworthy results with respect to the stack section and the determined attributes. In view of the authors, the proposed strategies offer an exciting approach to improve the stack section and to allow for a subsequent inversion and other applications like, e.g., the calculation of Fresnel zones or geometrical spreading factors.

Acknowledgments

This work was kindly supported by the *Wave Inversion Technology Consortium*, Karlsruhe, Germany and *Elf Exploration Production*, Pau, France.